Journal of
Synchrotron
Radiation

ISSN 0909-0495

Received 13 July 2004
Accepted 22 December 2004

Generalized prism-array lenses for hard X-rays

Björn Cederström,[a]* Carolina Ribbing[b] and Mats Lundqvist[a]

[a]Department of Physics, Royal Institute of Technology, SCFAB, SE-106 91, Stockholm, Sweden, and [b]Department of Engineering Sciences, Uppsala University, SE-751 21 Uppsala, Sweden.
E-mail: ceder@particle.kth.se

A Fresnel-like X-ray lens can be constructed by a triangular array of identical prisms whose base corresponds to the 2π-shift length. Each column of prisms is progressively shifted from the optical axis by an arbitrary fraction of the prism height. Similarly to the multi-prism lens, quasi-parabolic profiles are formed by a superposition of straight-line segments. The resulting projected lens profile is approximately linear with a Fresnel-lens pattern superimposed on it to provide the focusing. This geometry exhibits a significantly larger effective aperture than conventional parabolic refractive lenses. Prototype lenses were fabricated by deep reactive ion etching of silicon. These one-dimensionally focusing lenses were tested at a synchrotron beamline and provided focal line-widths down to 1.4 μm FWHM and an intensity gain of 39 at a photon energy of 13.4 keV. Fabrication imperfections gave rise to unwanted interference effects resulting in several intensity maxima in the focal plane. The presented design allows the focal length to be shortened without decreasing the feature size of the lens. Furthermore, this feature size does not limit the resolution as for real Fresnel optics.

Keywords: X-ray optics; refractive lenses; Fresnel lenses.

1. Introduction

In an early theoretical treatise on Fresnel and refractive X-ray lenses, the former were ruled more feasible owing to the unfavorable ratio of phase shift to absorption at X-ray wavelengths (Yang, 1993). Nevertheless, refractive X-ray lenses were the first to see the light owing to their ease of fabrication. The performance of this first generation of compound refractive lenses (CRLs) was limited by spherical aberration (Snigirev *et al.*, 1996). Later X-ray lens designs, such as one- or two-dimensionally focusing parabolic CRLs (Lengeler *et al.*, 1999) and one-dimensionally focusing multi-prism lenses (MPLs) (Cederström *et al.*, 2002), are spherical-aberration-free. Apart from fabrication imperfections, their aperture is restricted only by absorption in the lens. This intrinsic limitation can be mitigated by a choice of a low-Z lens material, such as lithium (Dufresne *et al.*, 2001; Pereira *et al.*, 2004), beryllium (Schroer *et al.*, 2002), plastics (Piestrup *et al.*, 2000) or diamond (Snigirev *et al.*, 2002; Ribbing *et al.*, 2003). However, for fabrication reasons, for example, aluminium (Lengeler *et al.*, 2002) and silicon (Aristov *et al.*, 1999) have frequently been employed. Schroer *et al.* (2003) achieved a focal spot size of 210 nm × 380 nm at 25 keV using crossed-planar short-focus silicon lenses, and similar results have been reported for planar SU-8 lenses at 14 keV (Snigirev *et al.*, 2003).

The natural solution to the absorption problem, to manufacture real Fresnel or Fresnel-like lenses, has only recently been successful. Planar Fresnel-like lenses (also known as kinoform lenses) were first etched in silicon (Aristov *et al.*, 2000) and later in diamond (Nöhammer *et al.*, 2003). The performance has so far not been able to match the best of the conventional refractive lenses, and focal line widths of a few micrometers (FWHM) are reported.

Recently, it was presented how a Fresnel-like lens can be built up of a pyramid of identical small parabolic structures by adding a parabolic correction to the Fresnel version of the multi-prism lens (Jark *et al.*, 2004). Lenses in SU-8 made by deep X-ray lithography provided a 2.8 μm focal line width at 8 keV, which is 50% larger than expected from theory. Imperfections of the lenses gave rise to several diffraction orders and a limited effective aperture.

This paper presents a more general modification of the multi-prism lens, which, while preserving the general structure, transforms the projected lens profile into an approximately linear shape on which a Fresnel-like pattern is superimposed. The basic idea of removing chunks of material corresponding to a phase shift of a multiple of 2π results in a structure shown schematically in Fig. 1.

The lenses described in this paper differ from those presented by Jark *et al.* (2004) in that the columnar shift along the y-axis can be any fraction of the prism height. If this

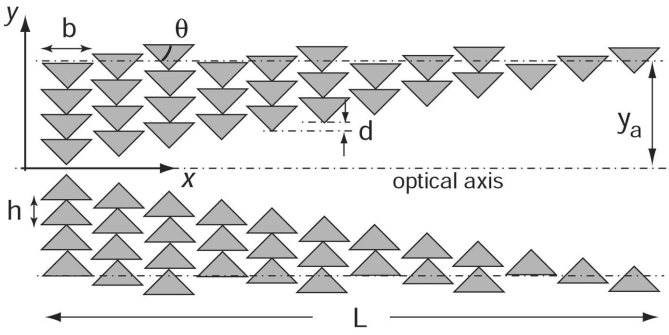

Figure 1
Schematic of one of many possible configurations of the prism array lens with the important parameters indicated.

fraction is sufficiently small, there is no need for a parabolic correction since each Fresnel zone is approximated by several straight-line segments. Furthermore, this makes the extension of the concept to higher energies and shorter focal lengths possible, while preserving the feature size of the prisms. This comes at the expense of a smaller aperture owing to absorption.

2. Theory

2.1. Projected lens profile

To analyze the lens in a physical optics perspective, we make a thin-lens approximation and calculate the projected lens profile, *i.e.* the integrated thickness of material at a certain height above the optical axis. Some basic definitions and geometrical relations are

$$\tan\theta = 2h/b, \quad y_a = Mh, \quad L = Nb, \tag{1}$$

where M is the number of prisms in the first column and N is the number of columns. The lens is comprised of approximately MN prisms. The phase condition is $b = q\lambda/\delta \equiv qL_{2\pi}$, where q is a positive integer, λ is the wavelength and δ is the deviation from unity of the real part of the index of refraction; $n = 1 - \delta + i\beta$.

The thickness of material in the first column at a lateral position y can be written as

$$x(y) = \mathrm{mod}(2y/\tan\theta, b), \tag{2}$$

where mod(...) is the modulus function (remainder after division). The ith column (starting at 0) is displaced a distance $id \equiv ih/\gamma$, where the important lens parameter γ is defined as the ratio of prism height to displacement. The thickness of material in the ith column is given by

$$x_i(y) = x(y - id) = \mathrm{mod}\left[\frac{2(y - id)}{\tan\theta}, b\right], \tag{3}$$

and the total path length is

$$X(y) = \sum_{i=0}^{\mathrm{div}(y,d)} x_i(y) = \sum_{i=0}^{\mathrm{div}(y,d)} \mathrm{mod}\left[\frac{2(y - id)}{\tan\theta}, b\right]. \tag{4}$$

Let us write $y = (j + t)d$, where j is an integer and $0 \le t < 1$. Then

$$\begin{aligned} X(j,t) &= \sum_{i=0}^{j} \mathrm{mod}\left[\frac{2d}{\tan\theta}(j + t - i), b\right] \\ &= \frac{d}{\tan\theta}[j(j+1) + 2(j+1)t] \\ &\quad - b\sum_{i=0}^{j} \mathrm{div}\left[\frac{2d}{\tan\theta}(i + t), b\right] \equiv X_0(j,t) - X'(j,t). \end{aligned} \tag{5}$$

Since the second term, $X'(j,t)$, in (5) cannot change the phase of the wave (other than by a multiple of 2π), it will not have any influence on the focusing, and we can disregard it for now.

2.2. Small-scale variation

The first term, $X_0(j,t)$, in (5) is the usual expression for the multi-prism lens profile (Cederström, 2002). The deviation from a parabola with apex in $y = -d/2$ is

$$\begin{aligned} n\delta X(j,t) &= (d/\tan\theta)\left[(j + t + 1/2)^2 - j(j+1) - 2(j+1)t\right] \\ &= (b/2\gamma)[1/4 + t(t-1)]. \end{aligned} \tag{6}$$

To quantify the influence on the focusing efficiency, we follow the standard approach for surface roughness (Aristov *et al.*, 1999), although this is only an approximation for non-Gaussian errors. We subtract the average phase shift and calculate the root-mean-square deviation (r.m.s.) over the segment,

$$\langle \delta X(t) \rangle_t = \frac{b}{2\gamma}\left[\int_0^1 (t^2 - t + 1/6)^2\, \mathrm{d}t\right]^{1/2} = L_{2\pi}\frac{q}{2(30^{1/2})\gamma}. \tag{7}$$

The r.m.s. deviation of the phase will be $\sigma_\varphi = \pi q/(30^{1/2}\gamma)$ and the intensity in the central peak will be reduced by a factor (first-order diffraction efficiency) $R = \exp(-\sigma_\varphi^2) \simeq \exp[-0.33(q/\gamma)^2]$. The ratio γ/q shows how well we approximate a Fresnel lens. As an example, $\gamma/q = 2$ gives $R = 0.92$.

The parabolic approximation gives

$$X_0(j) \simeq \frac{d}{\tan\theta}\, j^2 = \frac{y^2}{d\tan\theta} \simeq \frac{y^2}{2R}, \tag{8}$$

and [*cf.* Jark *et al.* (2004) who derive this for the special case $\gamma = 1$]

$$F = R/\delta = \frac{d\tan\theta}{2\delta} = \frac{q\lambda\tan^2\theta}{4\gamma\delta^2}. \tag{9}$$

2.3. Large-scale profile

The second non-phase-shifting term in (5) can be approximated by

$$\begin{aligned} X'(j,t) &= b\sum_{i=0}^{j} \mathrm{div}(i + t, \gamma) = b\sum_{i=t}^{j+t} \mathrm{div}(i, \gamma) \\ &\simeq \frac{d}{\tan\theta}\left[(j+t)^2 + j + t - \gamma(j+t)\right]. \end{aligned} \tag{10}$$

Using this approximation, the total profile can be written

$$X(j,t) = X_0(j,t) - X'(j,t) = \frac{d}{\tan\theta}\left[t - t^2 + (j+t)\gamma\right]. \quad (11)$$

Neglecting the small oscillating terms t and t^2 we finally have

$$X(y) \simeq \frac{\gamma}{\tan\theta}\, y \equiv Ky. \quad (12)$$

This shows that the large-scale profile is linear with the coefficient

$$K = \frac{b\tan\theta}{4\delta F} = \frac{q\lambda\tan\theta}{4\delta^2 F}. \quad (13)$$

This approximation can actually be derived from a simple geometric argument and by realising that half of the triangular lens is filled with material. We then have $K = (1/2)(b/d) = \gamma/\tan\theta$. For the special case $\gamma = 1$, this equation is not a good approximation [see Jark *et al.* (2004) for the correct expression for this case]. Projected lens profiles calculated from the exact expression in (5) and the approximation in (12) are shown in Fig. 2.

2.4. Transmission, effective aperture and intensity gain

The intensity transmission through the lens is $T(y) = \exp(-k|y|/l)$, where l is the attenuation length. The effective aperture, defined as the width of a slit that would transmit an equal amount of power, is then

$$D(y_a) = \int_{-y_a}^{y_a} \exp(-k|y|/l)\,\mathrm{d}y = D_\infty\left[1 - \exp(-2y_a/D_\infty)\right], \quad (14)$$

where

$$D_\infty = 2l/k = \frac{8\delta^2 lF}{q\lambda\tan\theta}. \quad (15)$$

As a practical rule of thumb, we could choose $y_a = D_\infty$, which would give 86% of the transmitted power provided by an infinitely large lens, while keeping a modest lens size.

Perfect imaging of a Gaussian source of width d_o at a distance s_o from the lens will give a peak intensity gain of

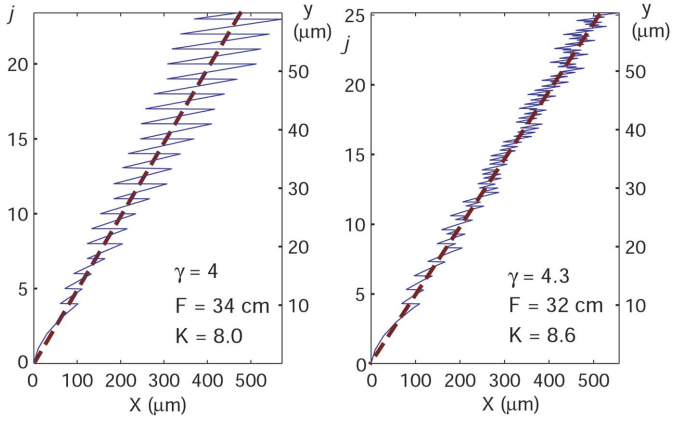

Figure 2
Projected lens profiles for different values of γ calculated from equation (5). Only a small part of the profiles is shown for clarity. The straight dashed line is the approximation of equation (12).

$$G = 0.94(s_o/s_i + 1)\, D/d_o, \quad (16)$$

where the distance from the lens to the focal plane, s_i, is given by Gauss' lens formula, $1/F = 1/s_o + 1/s_i$. In most synchrotron geometries we have $s_o \gg F$, in which case a good approximation is $G \simeq s_o D/(d_o F)$.

2.5. Comparison with parabolic refractive lenses

To see how much is to gain theoretically by this design, we recall that the effective aperture for CRLs and MPLs is given by $D_{\rm MPL} = (2\pi)^{1/2}\sigma_{\rm abs}$, where $\sigma_{\rm abs} = (\delta lF)^{1/2}$ is the r.m.s.-width of the Gaussian aperture (Lengeler *et al.*, 1999; Cederström *et al.*, 2002). We can form an aperture improvement factor (AIF) given by

$$\mathrm{AIF} = \frac{D_\infty}{D_{\rm MPL}} = 3.2\,\frac{\sigma_{\rm abs}}{qL_{2\pi}\tan\theta}. \quad (17)$$

Apart from the interesting dependence on material properties and energy, we see that both q and $\tan\theta$ must be minimized in order to gain as much as possible compared with ordinary refractive lenses. Fabrication capabilities may, however, constrain these variables.

2.6. Dependence on material and energy

To study the dependence on energy and lens material, we use a semi-empirical expression for the cross section as a function of energy and atomic number,

$$\sigma = 24.2\, Z^{4.2}E^{-3} + 0.56Z, \quad (18)$$

where E is in keV and σ is given in barns. The deviation from published data (Berger *et al.*, 2004) is less than 5% in the energy range 10–60 keV and for atomic number in the range 4–14.

Assuming low energy, the second term, corresponding to Compton scattering, can be neglected,

$$D \propto \frac{\delta^2 l}{\lambda} \propto \frac{\rho^2 E^{-4}\rho^{-1}Z^{-3.2}E^3}{E^{-1}} = \frac{\rho}{Z^{3.2}}. \quad (19)$$

Assuming high energy, the first term, corresponding to photoabsorption, can be neglected,

$$D \propto \frac{\delta^2 l}{\lambda} \propto \frac{\rho^2 E^{-4}\rho^{-1}}{E^{-1}} = \frac{\rho}{E^3}. \quad (20)$$

We can make a few interesting comparisons with ordinary refractive lenses:

(i) The material density plays a role, unlike the case for the MPL;

(ii) The dependence on atomic number is stronger than for the MPL;

(iii) There is no optimal energy. The aperture (gain) reaches a plateau for low energies.

2.7. Numerical example

As an example, we take a silicon lens with a focal length of 1 m. For silicon, $L_{2\pi} = 2.56\ \mu\mathrm{m\ keV}^{-1}\,E$. The effective aperture as a function of energy is shown in Fig. 3. Curves are given for different values of the prism angle θ, which should

obviously be kept as small as possible to optimize the performance. Also included is the effective aperture for a conventional refractive lens. The result would be significantly better with a lens material with lower atomic number. Diamond, for example, would have a 15 times larger effective aperture than silicon at $E = 20$ keV and $F = 1$ m.

3. Manufacturing

Owing to its favorable fabrication capabilities, silicon was chosen as the material for the first prototype lenses. Lenses with various prism sizes and angles were fabricated by deep reactive ion etching of silicon according to the so-called Bosch process (Laerme *et al.*, 1999). This is a plasma-based cyclic process with alternating etching and passivation steps, which can be used to attain microstructures with aspect ratios of up to 40:1. The process can be tuned for optimization of side-wall verticality and reduction of side-wall roughness. The prototype lenses described in this article were not fully optimized, but exhibited some remaining surface roughness and underetch at prism corners (Fig. 4). The base of the prisms (b) is 40 µm and the height (h) is 10 µm. The etch depth is 70–100 µm. The mask material, sputtered aluminium, was patterned using standard UV lithographic techniques with about 1 µm resolution. This introduced a certain amount of figure error, as evident from the connected prisms.

Lenses with $b = 25$ µm and $h = 5$ µm were also fabricated. In this case the process was unsuccessful and the columns were not separated.

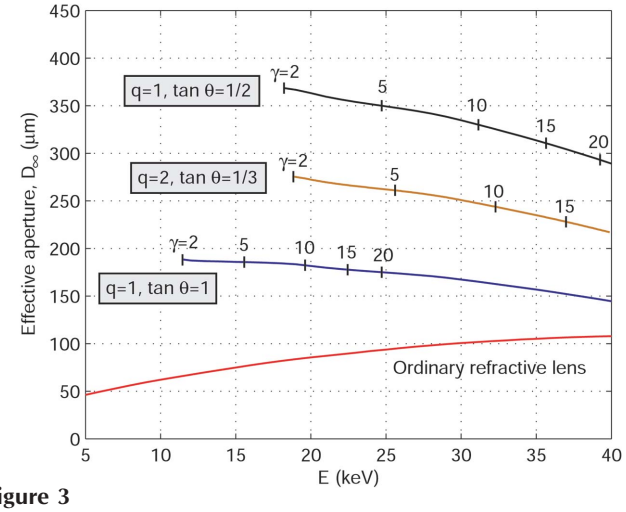

Figure 3
Effective aperture as a function of energy for a silicon prism-array lens with a focal length of 1 m. Three different lens designs are shown. Some values of γ are indicated along the curves. For comparison, the effective aperture of an ordinary refractive lens is also included.

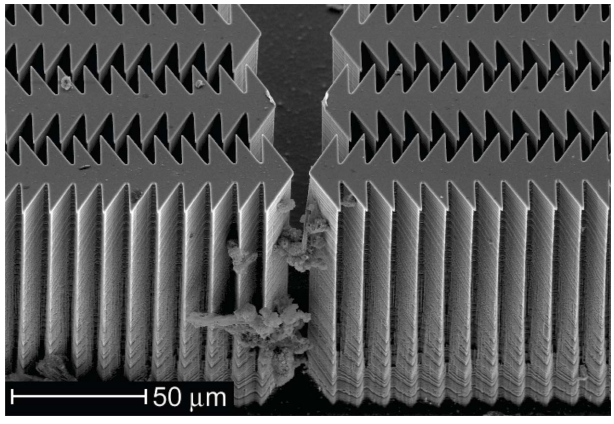

Figure 4
SEM image showing a silicon lens made using deep reactive ion etching. The aluminium etch mask is still present. Underetch and surface roughness is evident. The parameters for this lens are $b = 40$ µm, $h = 10$ µm, $\gamma = 2$.

4. Measurements

The prototype silicon lenses were tested at the optics evaluation beamline BM5 at the European Synchrotron Radiation Facility (ESRF) in May 2003. The lenses were focusing in the vertical direction and were placed 40 m from the source with a vertical size of 80 µm FWHM. A FReLoN X-ray CCD camera with a resolution of 1–2 µm was used for most measurements, while edge scans using a piezo-controlled tantalum knife-edge were used for high-resolution beam profiles.

All measurements presented here are for the lens depicted in Fig. 4 with design parameters $b = 40$ µm, $h = 10$ µm, $\gamma = 2$, $M = 40$, $F = 63$ cm at $E = 15.7$ keV. Using $\delta = 1.96 \times 10^{-6}$ and $l = 0.48$ mm, equations (14) and (15) give $D_\infty = 234$ µm and $D = 206$ µm for a vertical beam size of 0.5 mm. The intensity gain should be $G = 1.6 \times 10^2$.

Using the CCD camera, the narrowest focal line was found for $E = 14$ keV at a distance of 59 cm from the lens. The lower energy and shorter focal length are consistent with the underetch and hence smaller prisms than designed, as can also be seen in Fig. 4. The intensity map in the focal plane is shown in Fig. 5. The focal line has a width of 2.8 µm and the peak intensity gain is 18, *i.e.* substantially lower than expected from theory. This can partly be explained by the insufficient resolution of the CCD camera.

Several higher-order maxima appear in the focal plane and about 40% of the power is in the central peak. The period of the interference fringes is $P = 10$ µm or $\varphi = P/s_i = 18$ µrad in

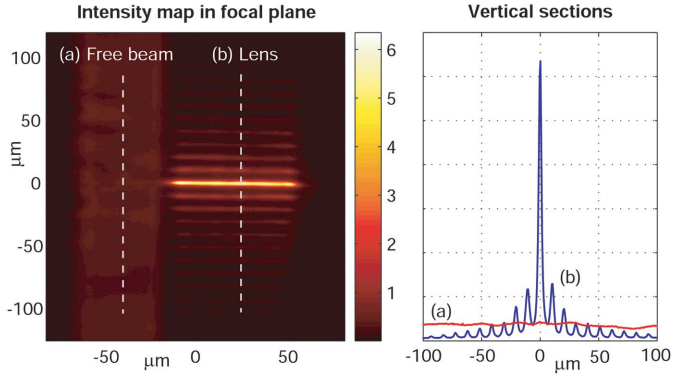

Figure 5
Intensity in the focal plane imaged by an X-ray CCD camera. Gain = 18, FWHM = 2.8 µm. The fraction of power in the central peak is 36%.

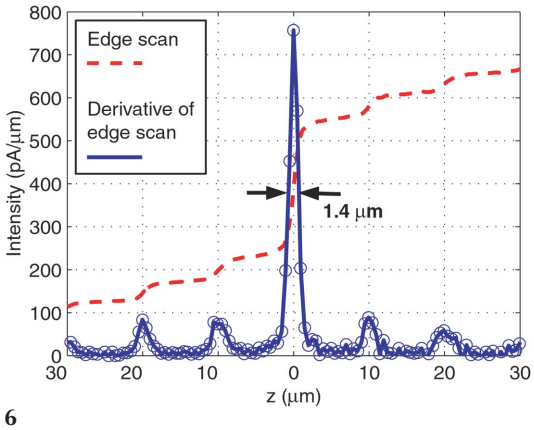

Figure 6
Intensity in focal plane measured with knife-edge scan. $E = 13.4$ keV, $F = 55$ cm, intensity gain = 39, FWHM = 1.4 μm, the fraction of power in the central peak is 41%.

angular units. This indicates a diffracting structure with periodicity $\lambda/\varphi = 5$ μm, which is exactly the columnar displacement $d = h/\gamma$. In fact, one can see in the SEM image a surplus of material at the center of the prisms of about 1/6 of the prism base b. However, in reality it is smaller owing to the underetch. Nevertheless, this results in out-of-phase contributions from the outer part of the lens, and only the innermost three to four rows of prisms contribute positively to the focusing. This could also be verified experimentally by reducing the beam vertically. This removed the interference peaks without much loss of central peak intensity.

For two-dimensional focusing using crossed lenses, it is important that the focal line is straight and regular. In this respect the results are very encouraging. We can define a line by the center points of Gaussian distributions fitted to the central peak for each CCD column independently. Across 60 μm the r.m.s. deviation from a straight line is only 0.04 μm, which should give a negligible broadening of the focal point for crossed focusing.

The result from an edge scan of the focal line is shown in Fig. 6. With the improved resolution, the focal line width is measured to 1.4 μm, which is close to the theoretical value of 1.1 μm. The peak intensity gain is 39 and the central peak contains 41% of the power. Here, the energy was adjusted to 13.4 keV and the image was found 54 cm from the lens.

5. Conclusions

It has been shown how a Fresnel-like X-ray lens can be built up of an array of identical prisms in a triangular arrangement. If the displacement of prism columns is sufficiently small compared with the prism height, no parabolic correction is needed. This design also allows short focal lengths and high X-ray energy while preserving the feature size of the lens. The first batch of silicon lenses made by deep reactive ion etching provided focal line widths down to 1.4 μm, which is only 30% wider than expected. Fabrication imperfections caused unwanted diffraction effects and higher-order maxima in the focal plane, which limited the intensity gain to 39 for planar focusing. This is likely to be improved with optimized lens fabrication.

This work was funded by the Swedish Foundation for Strategic Research, ALMI Business Partner, the Göran Gustafsson Foundation and Uppsala University Industrial Liaison Office. We acknowledge the European Synchrotron Radiation Facility for provision of synchrotron radiation facilities and we would like to thank Joanna Hoszowska for assistance in using beamline BM5.

References

Aristov, V., Grigoriev, M., Kuznetsov, S., Shabelnikov, L., Yunkin, V., Weitkamp, T., Rau, C., Snigireva, I., Snigirev, A., Hoffmann, M. & Voges, E. (2000). *Appl. Phys. Lett.* **77**, 4058–4060.
Aristov, V. V., Starkov, V. V., Shabelnikov, L. G., Kuznetsov, S. M., Ushakova, A. P., Grigoriev, M. V. & Tseitlin, V. M. (1999). *Opt. Commun.* **161**, 203–208.
Berger, M. J., Hubbell, J. H., Seltzer, S. M., Coursey, J. S. & Zucker, D. S. (2004). XCOM: Photon Cross Sections Database (Version 1.2), http://physics.nist.gov/xcom.
Cederström, B. (2002). *A Multi-Prism Lens for Hard X-rays.* Stockholm: Royal Institute of Technology.
Cederström, B., Ribbing, C. & Lundqvist, M. (2002). *Appl. Phys. Lett.* **18**, 121–123.
Dufresne, E. M., Arms, D. A., Clarke, R., Pereira, N. R., Dierker, S. B. & Foster, D. (2001). *Appl. Phys. Lett.* **79**, 4085–4087.
Jark, W., Perennès, F., Matteucci, M., Mancini, L., Montanari, F., Rigon, L., Tromba, G., Somogyi, A., Tucoulou, R. & Bohic, S. (2004). *J. Synchrotron Rad.* **11**, 248–253.
Laerme, F., Schilp, A., Funk, K. & Offenberg, M. (1999). *Technical Digest MEMS'99*, pp. 11–216. IEEE Robotics and Automation Society.
Lengeler, B., Schroer, C., Benner, B., Gerhardus, A., Florian, T., Günzler, T. F., Kuhlmann, M., Meyer, J. & Zimprich, C. (2002). *J. Synchrotron Rad.* **9**, 119–124.
Lengeler, B., Schroer, C., Tümmler, J., Benner, B., Richwin, M., Snigirev, A., Snigireva, I. & Drakopoulos, M. (1999). *J. Synchrotron Rad.* **6**, 1153–1167.
Nöhammer, B., Hoszowska, J., Freund, A. & Somogyi, A. (2003). *J. Phys. IV Fr.* **104**, 223–226.
Pereira, N. R., Dufresne, E. M., Clarke, R. & Arms, D. A. (2004). *Rev. Sci. Instrum.* **75**, 37–41.
Piestrup, M. A., Cremer, J. T., Beguiristain, H. R., Gary, C. K. & Pantell, R. H. (2000). *Rev. Sci. Instrum.* **71**, 4375–4379.
Ribbing, C., Cederström, B. & Lundqvist, M. (2003). *Diam. Relat. Mater.* **12**, 1793–1799.
Schroer, C., Kuhlmann, M., Hunger, U. T., Günzler, T. F., Kurapova, O., Feste, S., Frehse, F., Lengeler, B., Drakopoulos, M., Somogui, A., Simionovici, A. S., Snigirev, A., Snigireva, I. & Schug, C. (2003). *Appl. Phys. Lett.* **82**, 1485–1487.
Schroer, C., Kuhlmann, M., Lengeler, B., Günzler, T., Karapova, O., Benner, B., Rau, C., Simionovici, A., Snigirev, A. & Snigireva, I. (2002). *Proc. SPIE*, **4783**, 10–18.
Snigirev, A., Kohn, V., Snigireva, I. & Lengeler, B. (1996). *Nature (London)*, **384**, 49–51.
Snigirev, A., Snigireva, I., Drakopoulos, M., Nazmov, V., Reznikova, E., Kuznetsov, S., Grigoriev, M., Mohr, J. & Saile, V. (2003). *Proc. SPIE*, **5195**, 21–31.
Snigirev, A., Yunkin, V., Snigireva, I., Di Michiel, M., Drakopoulos, M., Kouznetsov, S., Shabelnikov, L., Grigoriev, M., Ralchenko, V., Sychov, I., Hoffmann, M. & Voges, E. (2002). *Proc. SPIE*, **4783**, 1–9.
Yang, B. X. (1993). *Nucl. Instrum. Methods Phys. Res. A*, **328**, 578–587.